ORIGINAL PAPER

Cobalt telluride electrocatalyst for selective electroreduction of CO_2 to value-added chemicals

Apurv Saxena[1] · Harish Singh[1] · Manashi Nath[1]

Abstract

Recent emphasis on carbon dioxide utilization has necessitated the exploration of different catalyst compositions other than copper-based systems that can significantly improve the activity and selectivity towards specific CO_2 reduction products at low applied potential. In this study, a binary CoTe has been reported as an efficient electrocatalyst for CO_2 reduction in aqueous medium under ambient conditions at neutral pH. CoTe showed high Faradaic efficiency and selectivity of 86.83 and 75%, respectively, for acetic acid at very low potential of -0.25 V vs RHE. More intriguingly, C1 products like formic acid was formed preferentially at slightly higher applied potential achieving high formation rate of 547.24 µmol cm^{-2} h^{-1} at -1.1 V vs RHE. CoTe showed better CO2RR activity when compared with Co_3O_4, which can be attributed to the enhanced electrochemical activity of the catalytically active transition metal center as well as improved intermediate adsorption on the catalyst surface. While reduced anion electronegativity and improved lattice covalency in tellurides enhance the electrochemical activity of Co, high d-electron density improves the intermediate CO adsorption on the catalyst site leading to CO_2 reduction at lower applied potential and high selectivity for C_2 products. CoTe also shows stable CO2RR catalytic activity for 50 h and low Tafel slope (50.3 mV dec^{-1}) indicating faster reaction kinetics and robust functionality. Selective formation of value-added C_2 products with low energy expense can make these catalysts potentially viable for integration with other CO_2 capture technologies thereby, helping to close the carbon loop.

Keywords CO_2 electrochemical reduction · CO_2 utilization · Formic acid production · Elecrocatalysts · Cobalt telluride

Introduction

Continuous usage of fossil fuels along with advent of the industrial age has led to catastrophic levels of CO_2 in the atmosphere which has skyrocketed after the industrial revolution, reaching 401.3 parts per million in 2015 from approximately 270 ppm in the pre-Industrial revolution era [1, 2]. Unfortunately atmospheric CO_2 levels are expected to rise even further and exceed 600 parts per million by the end of the twenty-first century [1–4]. Development of techniques for reducing the level of atmospheric carbon dioxide has become very crucial given the catastrophic effects of global warming [1]. These techniques are broadly categorized into CO_2 sequestration, storage and utilization which can be integrated with direct air capture (DAC). Among

these, electrochemical CO_2 reduction reaction (CO2RR) is one of the most promising CO_2 utilization strategies. CO_2 electroreduction is most viable among other carbon dioxide conversion technologies such as biochemical, photosynthetic, thermo-catalytic, and photocatalytic processes, due to mild electrolyzer operating conditions, selectivity toward the desired products, and ambient condition operation [5, 6]. Inspiration for this technique can be derived from photosynthesis process which meticulously converts CO_2 to maintain proper balance of atmospheric gases. Carbon dioxide has two carbon-oxygen double bonds with a total bond energy of 750 kJ mol^{-1} which makes it extremely challenging to bring it out of the potential well [7]. Hence a catalyst is required to reduce CO_2 to other products by reducing the activation energy through effective catalyst-mediated charge transfer [3]. Electrochemical conversion is an environment friendly way of supplying that energy due to its mild operation conditions and renewable sources of electricity. Hori et al. reported some pioneering research on carbon dioxide electroreduction using various transition metals like Pb, Hg,

✉ Manashi Nath
nathm@mst.edu

[1] Department of Chemistry, Missouri University of Science and Technology, Rolla, MO 65409, USA

In, Sn etc. and Cu, Au, Ag, Pt etc. which led to the formation of formate and CO, respectively, as the reduction products. However, through subsequent research it was also found that lot of these metal catalysts had other disadvantages, such as poor selectivity towards specific reduction products, were environmentally toxic and frequently underwent poisoning [8]. Intense research activities over the last several years has led to identification of catalysts with better selectivity and activity achieved through modulating catalyst morphology and dimensionality [9, 10], vacancy creation [11], and doping [12–15]. However, it must also be noted that majority of the catalysts reported for CO2RR were Cu-based compositions [4, 16–19]. There have been very few reports of electrocatalysts for CO2RR based on Fe, Co, and/or Ni based compositions [20]. Among these, Co-based catalysts have been previously used in industry for various processes like Fisher–Tropsch synthesis [21–23], and electrocatalytic water splitting [24]. Co-based compositions exhibit unique properties like enhanced conductivity and electrochemical tunability which makes them suitable for CO_2 electroreduction. Indeed some Co-based catalysts have been reported for CO2RR, specifically as Co SACs (single atom catalyst) [18, 19, 25–28], Co-MOFs [29–32], Co-coordination complexes, cobalt-based nitrides [33–35], and oxides [28, 36–39]. Cobalt exhibits better CO2RR activity due to factors like optimal CO_2 adsorption energy and low energy difference between Co d-band and Fermi level [40]. Also, it has been observed that during the CO_2 reduction Co^{2+} converts to Co^+. This transition happens during the rate-determining step which results in selectivity towards products and enhances activity and stability of the catalyst [41, 42]. Co SAC has been found to be highly selective towards CO with Faradaic efficiency (FE) of 95% with current density towards CO production being 86.4 mA cm^{-2}. This is significant improvement from the Cobalt metal-based catalyst [27]. Cobalt nanoparticles dispersed on NrGO developed through a one-step synthesis was found to be selective towards methanol with high faradaic efficiency of 71.4% at −0.9 V vs SCE [43]. Co single atoms anchored on Te nanosheets showed efficient electron transfer leading to efficient photocatalytic CO_2 conversion [44]. Co_3O_4 nanofiber modified electrodes has been found to have good activity towards CO2RR having high faradaic efficiency for both CO and formate (90%) [45]. Ultrathin Co_3O_4 layers of 1.72 and 3.51 nm thickness exhibited 64.3% Faradaic efficiency at −0.88 V vs. SCE with superior structural stability [38]. Cobalt phthalocyanine exhibited very high activity towards CO_2 conversion when phthalocyanine was modified by trimethyl ammonium. This catalyst reduces CO_2 to CO with selectivity of 95% over a wide range of pH (4–14) [46]. A hydrothermally synthesized core–shell structured Co_3S_4@Co_3O_4 catalyst show high selectivity towards formic acid with FE of 85.3% [47].

In all these electrocatalysts, transition metal serves as the catalytic center for CO2RR where the reaction progress via intermediate steps involving adsorption of O-containing intermediates [48]. Hence, it can be expected that tuning the electron density around the transition metal center will influence adsorption of reaction intermediates and resulting charge transfer rate, leading to reduction of overpotential for electrocatalytic CO2RR. Previously, we have shown that changing anion electronegativity leads to modulation of d-electron density around transition metal center [6]. More specifically, we have shown that reducing anion electronegativity leads to better electrocatalytic activity making selenides and tellurides as better electrocatalysts with lower overpotential [6, 17, 49]. Similar observation was made in Cu-based systems, where Cu_2Se was observed to exhibit lower overpotential for CO2RR compared to Cu or CuO [17]. While lower overpotential is a measure for enhanced catalytic activity, for CO2RR, the additional criteria for improved activity is selectivity for formation of specific reduction products and the ability to form carbon-rich value-added products with high Faradaic efficiency. We have proposed that selectivity towards C_{2+} reduction products depend critically on the adsorption energy and dwell time of intermediate *CO on the catalyst site, which in turn depends on the d-electron density of the transition metal as well as electronegativity of the coordinated anions. In this article, we have described CoTe nanostructures as a new family of metal chalcogenide electrocatalysts for the CO2RR with high selectivity for forming C_2 reduction products at low applied potential and neutral pH. Apart from enhanced catalytic activity, these CoTe nanostructures also showed high faradaic efficiency, and long-term functional stability. Also, because of the extensive stoichiometry alterations that are possible in metal-rich chalcogenides, these materials are highly efficient, inexpensive, and robust electrocatalysts for a variety of electrochemical sensors, energy conversion, and storage applications [49–52].

Experimental

Materials

All the reagents were of analytical grade and used as received. Deionized water (resistivity 18 MΩ cm) was used to prepare all solutions. Cobalt sulfate ($CoSO_4$·$6H_2O$) was purchased from Sigma–Aldrich; hydrazine hydrate (N_2H_4·H_2O, 100%), and tellurium dioxide (TeO_2) were purchased from Acros Organics. Nafion and carbon fiber paper (CFP) substrate were obtained from Fuel Cells, etc., in College Station, Texas.

Synthesis of CoTe

CoTe was prepared by hydrothermal technique as reported previously [24]. Specifically, an equimolar ratio (1:1) of cobalt sulfate ($CoSO_4 \cdot 6H_2O$) and tellurium dioxide (TeO_2) powder was used for the synthesis. Initially the $CoSO_4 \cdot 6H_2O$ was dissolved in 9 mL of deionized water in a Teflon-lined stainless-steel autoclave with a capacity of 23 mL. After vigorous stirring for 20 min, TeO_2 was added to the mixture. Finally, 3 mL of $N_2H_4H_2O$ were added to the mixture, which was continually stirred for another 30 min. The resultant solution was placed in a teflon lined stainless-steel autoclave. The autoclave was sealed and kept at 145 °C for 24 h before being allowed to cool naturally to room temperature. The resulting product was centrifuged and rinsed several times with an ethanol/deionized water mixture. The final product was dried at 60 °C in a vacuum oven.

Characterization

Powder X-ray diffraction (PXRD) patterns were obtained using a Philip X-Pert powder X-ray diffractometer using Ni-filtered Cu–K radiation with a wavelength of 1.5406, within the 20°–90° range. Morphology of the as-prepared sample was examined using an FEI Helios Nanolab 600 scanning electron microscope with a working distance of 10 mm and a 15 kV acceleration voltage. A Tecnai F20 was used to acquire TEM images of the synthesized samples directly on the formvar-coated Cu grid. Additionally, the surface chemical composition was analyzed using X-ray Photoelectron Spectroscopy (XPS) with a KRATOS AXIS 165 spectrometer equipped with an Al X-ray source. To examine the true surface chemistry, all XPS data were acquired without sputtering.

Electrochemical measurements

To conduct the electrochemical measurements, an IviumStat potentiostat was used with graphite rod, Ag|AgCl (KCl-saturated) and carbon cloth as counter, reference and working electrode, respectively. All electrochemical experiments were performed in a H-cell at ambient temperature. Nafion membrane-117 proton exchange membrane was used to separate the anodic and cathodic compartments of H Cell. The electrochemical activity of catalyst was measured using a 3-electrode system where CoTe-modified carbon cloth was used as the working electrode. The Ag|AgCl reference electrode was calibrated with a Pt wire in H_2-saturated H_2SO_4 and an open circuit potential was obtained as -0.199 V. The potential reported vs Ag|AgCl was changed to reversible hydrogen electrode (RHE) using the following equation:

$$E_{RHE} = E_{Ag|AgCl} + 0.059pH + E^0_{Ag|AgCl} \tag{1}$$

where E_{RHE} is the transformed potential vs RHE. $E_{Ag|AgCl}$ is the experimentally obtained potential. $E^0_{Ag|AgCl}$ is the standard potential of Ag|AgCl (0.199 V). The pH of CO_2 saturated 0.3 M $NaHCO_3$ was estimated to be 6.8. Catalyst ink was made by sonicating 5 mg of hydrothermally synthesized CoTe in 500 μL of 1% Nafion in isopropanol. The ink was then drop-casted on carbon fiber papercloth to make working electrode. Measured potentials vs Ag|AgCl were converted to RHE for accurate comparison and data interpretation. Before starting the electrochemical reduction, the electrolyte was purged vigorously with CO_2 for 20 min and the flow was then tuned down to ~ 10 mL min^{-1} during CO_2RR. To gauge CO_2 electrochemical reduction capability of electrocatalysts, different electrochemical experiments were performed on drop-casted working electrodes. The working electrode consists of catalyst and Nafion binder mixture deposited on one side of the carbon cloth (CC). Carbon fiber paper is a microporous substrate having pores of size between 1 and 100 μm. This type of substrate improves mechanical strength, electrical conductivity, and mass transport during CO_2 electroreduction. The Nafion helps in the catalyst utilization by increasing the ionic connection and increases water content in the pores because of its hydrophilic nature. Hence, catalyst mixture in form of microporous layer improves the interfacial electrical conductivity and inhibits electrolyte flooding [53].

Results and discussion

The phase purity and crystallinity of the hydrothermally synthesized samples were confirmed using PXRD patterns. Figure 1a shows the PXRD pattern of the hydrothermally synthesized product, which confirms crystallinity of the as-synthesized product and is well matched with the CoTe standard diffraction pattern (PDF No. 00-034-0420), demonstrating that the product was pure cobalt telluride. SEM and TEM were used to examine the morphology of the as-synthesized material. SEM and TEM images of hydrothermally produced CoTe are shown in Fig. 1b, c which shows that short nanorods with an average length of around 400 nm were formed in hydrothermally synthesized CoTe. To achieve high catalytic activity, it is desirable to use nanostructured morphology, because they have a large surface area and mass to volume ratio. Hence, the nanostructured morphology for CoTe seems to be advantageous for CO2RR catalytic activity. XPS studies were also used to confirm surface composition of the catalyst. The XPS spectra of hydrothermally produced CoTe are shown in
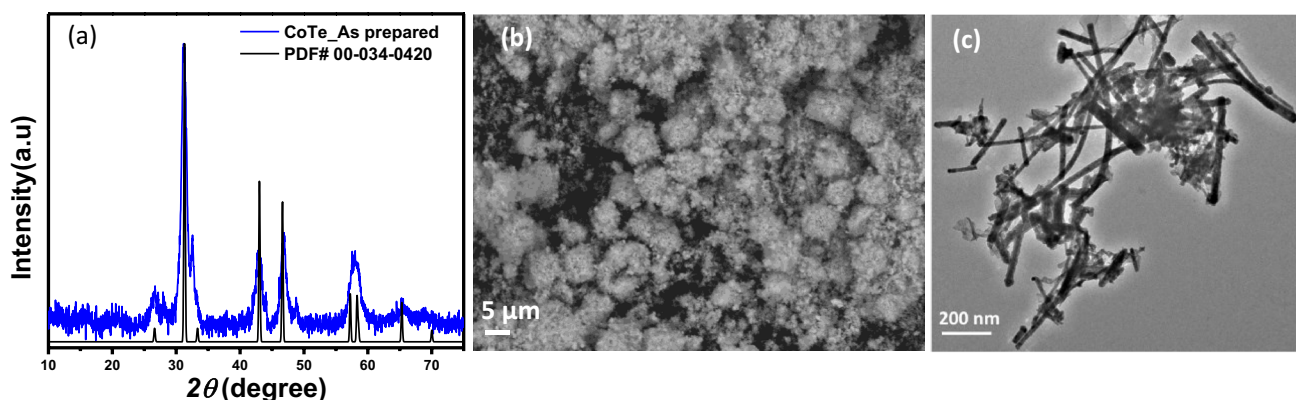
Fig. 1 **a** Powder X-ray diffraction pattern of CoTe compared with the standard. **b** SEM and **c** TEM of images of as-synthesized CoTe
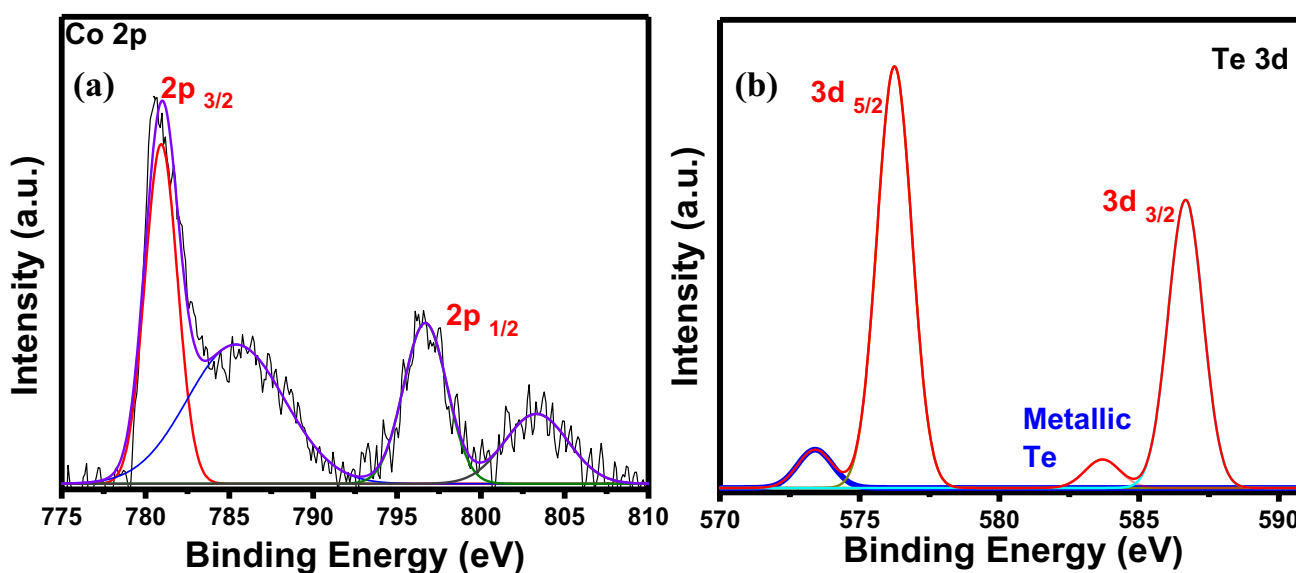

Fig. 2 XPS spectra of CoTe showing **a** Co 2p and **b** Te 3d peaks

Fig. 2. The Co 2p and Te 3d spectra are shown in Fig. 2a, b. Co 2p spectra exhibits two peaks at 780.4 and 795.8 eV, which correspond to 2p3/2 and 2p1/2, respectively, and are comparable to Co^{2+} [24]. The satellite peaks were found at 786.6 and 803.0 eV, which are consistent with the existing literature [24, 54]. Metallic Te was present in the Te XPS spectra at 572.8 and 583.3 eV. The XPS spectra also confirmed formation of CoTe in pure phase.

Electrocatalytic CO2RR performance of CoTe catalyst

In this study, all electrochemical measurements for studying CO2RR along with product detection and quantification has been performed by following standard protocol as has been reported previously including design of experimental set-up and measurement techniques [16, 55]. Moreover,

performance of our electrochemical set-up was calibrated and verified by measuring the CO2RR activity of standard polycrystalline Ag electrode and comparing it with previous reports. Products of CO2RR were found to be formic acid and CO at −0.9 V (vs RHE) on Ag electrode as shown in Figure S1, which is similar to that reported by previous researchers [8, 56], confirming the reliability of our electrochemical set-up for CO2RR studies. Observed current density from the LSV polarization curves were also similar to the reported studies which further confirms the validity of the experiments [57, 58]. Comparison of the CoTe-modified electrode with that of polycrystalline Ag, shows that different CO_2 reduction products were identified with CoTe-modified electrode under similar conditions, further corroborating the novelty of this catalyst. Details of CO2RR studies with CoTe-modified electrode have been discussed in the following sections.
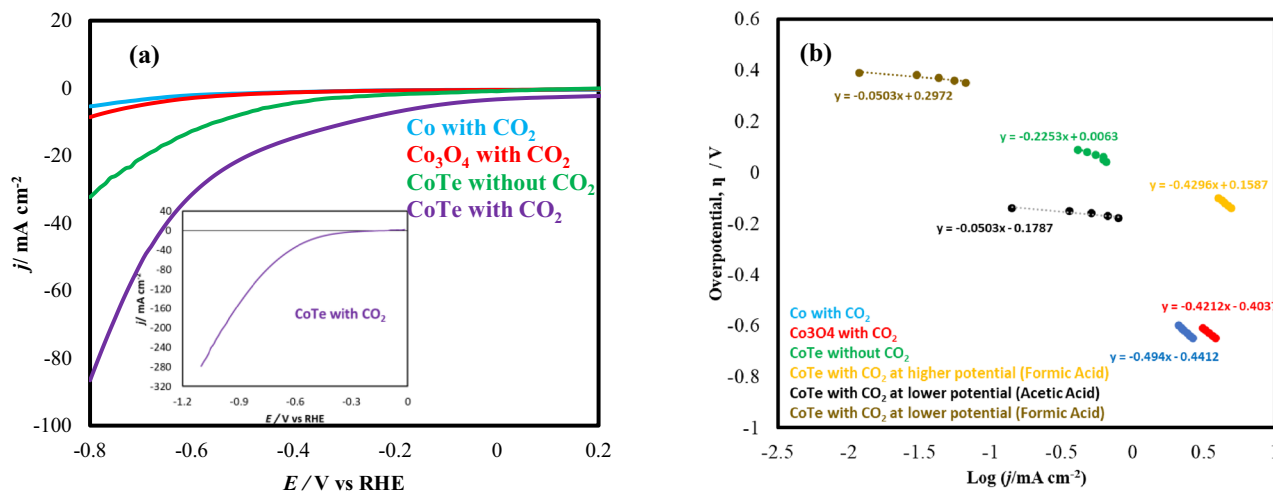
Fig. 3 **a** Comparison of LSVs measured in 0.3 M NaHCO$_3$ at a scan rate of 10 mV s^{-1} in the presence and absence of CO$_2$ with CoTe, Co, and Co$_3$O$_4$ modified GC electrodes. Inset shows the LSV scan of CoTe electrode till −1.1 V in the presence of CO$_2$. **b** Tafel plots of various electrodes measured in 0.3 M NaHCO$_3$ with and without CO$_2$

Linear scan voltammetry (LSV) was carried out in CO$_2$ or N$_2$ saturated 0.3 M NaHCO$_3$ at a 10 mV/s scan rate. On applying negative potential in N$_2$ saturated electrolyte only hydrogen evolution (HER) takes place, however, in CO$_2$-saturated electrolyte CO2RR and HER both occur simultaneously. As shown in Fig. 3, CoTe exhibited higher current density in CO$_2$-saturated electrolyte than in N$_2$-saturated electrolyte at the same potentials, confirming that the CoTe electrodes are active for CO2RR. CoTe achieved a CO2RR reduction current density of 278 mA cm^{-2} at −1.1 V vs RHE as shown in inset of Fig. 3 which is significantly higher than the current density exhibited by bulk Co, Co$_3$O$_4$ and the partially oxidized bulk Co [28, 45].
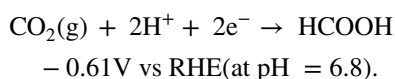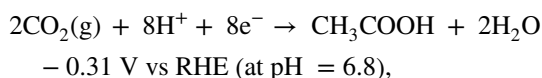
Tafel plot

The Tafel analysis can be an effective tool for explaining the electrokinetic activity of the electrocatalysts for CO2RR via Tafel slopes. The Tafel equation illustrates the relation between overpotential η with the current density j as shown in the following equation:

$$\eta = \alpha + (2.3RT) \log j / \alpha nF, \qquad (2)$$

where α represents the transfer coefficient, n is the number of electrons passed during the reaction, and F is the Faraday constant. The Tafel slope is calculated by 2.3$RT/\alpha nF$. The Tafel plots in this work were calculated from the LSV collected at a scan rate of 2 mV s^{-1} in a non-stirred N$_2$-saturated 1.0 M KOH solution. Data for the Tafel equation are obtained from the kinetically controlled range of CO$_2$ electrochemical reduction which determines the relation between

of overpotential η and current density j. The Tafel slope is crucial in measuring electrochemical performances, and it gives insights into the kinetics in the electrochemical reduction. Typically, lower Tafel slopes for a catalyst indicates faster CO2RR kinetics in a bicarbonate electrolyte. Tafel slope polarization curves were measured in continuously purged and stirred electrolyte solution at a lower scan rate of 2 mV s^{-1} to minimize mass transfer limitations. The Tafel plots of CoTe are shown in Fig. 3b. Since CO2RR is a multi-product reaction, Tafel analysis for CoTe-modified electrolyte in the presence of CO$_2$ was done at two different potentials to represent the two major products acetic acid and formic acid formed in this reaction. Specifically, Tafel analysis at low negative potential (−0.25 V) was performed with help of partial current density corresponding to acetic acid and formic acid formation. Tafel analysis at higher negative potential (−1.1 V) provided details for formic acid production which was the sole reduction product formed at that potential. Tafel slope of CoTe in the presence of CO$_2$ was estimated to be 50.3 mV dec^{-1} for both acetic acid and formic acid −0.25 V but at higher negative potential (−1.1 V) Tafel slope was observed to be 429.6 mV dec^{-1} for formic acid production. In the absence of CO$_2$, it showed a much higher Tafel slope of 225.3 mV dec^{-1}. The lower Tafel slope for formation of acetic acid at lower applied potential indicates faster reduction kinetics for formation of carbon-rich products highlighting novelty of this catalyst. The very low Tafel slope also indicates faster kinetics for the reduction of CO$_2$ in a bicarbonate electrolyte. The Tafel slope for CoTe is near to the theoretical value of 118 mV dec^{-1}, which is expected for the chemical rate-determining step (RDS) of initial single-electron transfer step for formation of

adsorbed radical intermediate ($CO_2^{·-}$) on the catalyst surface which initiates the catalytic CO_2 reduction [59, 60]. Lower Tafel slope values indicating faster intermediate adsorption kinetics on CoTe-modified electrode at lower applied potential also corroborates well with formation of CO_2 reduction products at lower applied potential including selective formation of carboxylic acids such as acetic acid as discussed below. The standard reduction potential of CO_2 to acetic acid is 310 mV vs RHE at neutral pH [61]. The standard potential for formic acid and acetic acid formation from CO_2 reduction (at neutral pH) as shown below was used for calculating the overpotentials at lower and higher negative potentials [61]:

$$2CO_2(g) + 8H^+ + 8e^- \rightarrow CH_3COOH + 2H_2O$$
$$-0.31 \text{ V vs RHE (at pH} = 6.8),$$

$$CO_2(g) + 2H^+ + 2e^- \rightarrow HCOOH$$
$$-0.61 \text{V vs RHE(at pH} = 6.8).$$

The low Tafel slope (50.3 mV dec^{-1}) measured near low overpotential of 310 mV indicates faster kinetics for acetic acid generation illustrating high selectivity and efficiency of the catalyst. However, given the complexity of CO2RR on the catalyst surface and multitude of steps, more studies are needed to correctly ascertain the proper RDS as well as accurate mechanism for CO2RR on the surface of CoTe. The Tafel slope for CoTe@CFP was observed to be smaller than

that of bare Co and Co_3O_4 which confirms the contribution of chalcogenides in fast transfer of electrons.

CO2RR products identification and quantification

The carbon dioxide reduction products were identified and quantified by performing chronoamperometric studies at constant applied potentials of -0.25, -0.6, -0.9, -1.1 V vs RHE in CO_2 purged $NaHCO_3$ to study the effect of applied potential on product composition and selectivity, if any. The products were collected from the cathodic chamber after 1 h of chronoamperometry at each fixed applied potential while the catholyte was subjected to constant purging with CO_2 gas at low flow rate (20 sccm). Identification and quantification of liquid products were done by ^{1}H NMR while gaseous products were detected and quantified using GC-TCD. From NMR plots as shown in Fig. 4a, it was observed that the product composition was very dependent on the applied potential and showed selectivity towards specific products at each potential. The Faradaic efficiency for formation of specific product was estimated from absolute product quantity obtained through NMR (Fig. 4b) and GC-TCD (Fig. 5) measurements, and using standard procedure as described previously [16, 55]. Interestingly, reduction products generated at low applied potentials (-0.25 to -0.6 V vs RHE) contained predominantly carbon-rich compounds like acetic acid, while at higher applied potential, C1 products such as formic acid were obtained with higher yield. At -0.25 V vs RHE, yield of formic acid was low probably due to low
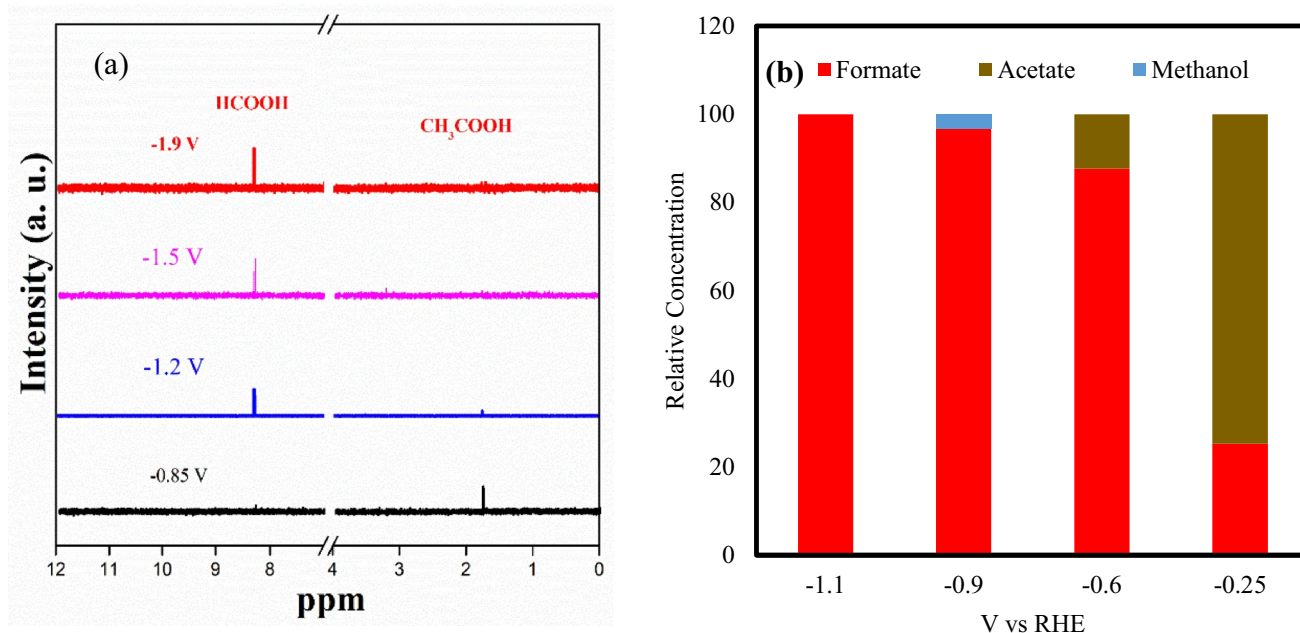

Fig. 4 **a** NMR spectra identifying CO_2 reduction products in reaction aliquots collected at different potentials. **b** Bar plot illustrating relative concentrations of liquid products quantified from NMR at different stationary applied potentials

Fig. 5 Bar plots depicting relative faradaic efficiency of cumulative liquid and gas phase CO_2 reduction products at different applied potentials quantified through NMR and GC-TCD
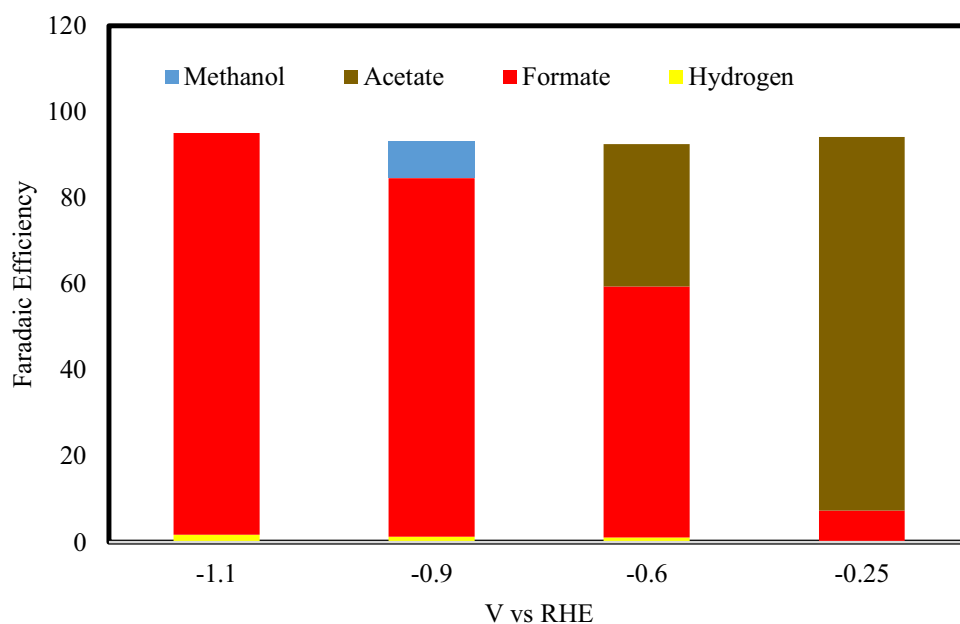
current density. Previous studies have reported that when pH decreases in the vicinity of the electrode surface due to continuous hydrogen evolution [62], in situ conversion of CO_2 to HCO_3^- occurs. However, this spontaneous change happens at higher concentration of nascent hydrogen which also leads to formation of formic acid at higher applied potential. Formic acid becomes a major product at -0.6 V with relative concentration of 86.25% and FE = 58.34%. When the applied potential was increased further, FE of formic acid reached maximum (93.39%) at -1.1 V vs RHE. Due to high HER activity and more hydrogen generation at higher applied potential, Faradaic efficiency of formic acid formation was found to decrease at further negative potential (<-1.1 V) [63]. CoTe exhibited high faradaic efficiency of formate production over 85% under a broad range from -0.9 to -1.1 V vs RHE and acetate production at -0.25 V vs RHE. This observation confirms the enhanced efficiency of CoTe catalyst which requires lower potential for CO2RR and exhibits a higher FE for high-value products such as formic and acetic acid than any other Co-based catalyst at similar applied potential. It must be noted here that the product composition was predominantly acetic acid at lower potential range near -0.25 V vs RHE. Such high selectivity towards formation of acetic acid with low energy expense has been rarely observed with CO2RR catalyst. Acetic acid is an industrially important chemical, and the selectivity towards its production at lower applied potential highlights the novelty of this catalyst. Specifically, this catalyst paves the way for high-selectivity direct acetic acid synthesis from CO_2 replacing the conventional multi-step industrial process which typically begins with synthesis of syngas and ends with the generation of methanol followed by its carbonylation [63]. Quantification

of hydrogen evolved during the reaction showed FE of 1.71, 1.23, and 1.03% at -1.1, -0.9, and -0.6 V vs RHE, respectively, as shown in Fig. 5. The observed product selectivity towards C1 and C2 products as opposed to H_2 also suggests that at lower applied potential intermediate adsorption and kinetics of CO2RR on the catalyst surface is more favorable than rate of water reduction. Moreover, the absence of CO in the product composition and preferential formation of exclusive C1/C2 products, makes CoTe catalyst very unique as almost all copper-based and other conventional CO2RR electrocatalyst are known to produce CO as their main product [64].

Previously Co-based catalyst has been reported for CO2RR producing formic acid as the major product. In this study, we have observed that when the catalytically active Co^{2+} is placed in the covalently bonded network of Te ions, electrochemical CO_2 reduction tends to yield more C2 products at lower potential. The results from our study will help to improve the existing and future catalyst compositions. Especially, once the influence of CoTe dense packed structures and effect of telluride on covalency is mechanistically studied.

The functional stability of the CoTe electrocatalyst for long-term hydrocarbon generation is also a critical factor in evaluating catalyst performance, applicability, and performance. Operational stability of CoTe for CO2RR was investigated by performing chronoamperometric study at different applied potentials for extended period of time. It should be noted that no change in the current density and Faradaic Efficiency was observed at -0.25, -0.6, -0.9, and -1.1 V, and CoTe exhibited exceptional functional stability for over 50 h of CO2RR activity as shown in Figure

S2. Moreover, NMR analysis of the aliquots collected every 10 h during the 50 h period showed that there was no change in product composition during this time confirming high degree of operational stability and minimal catalyst surface poisoning with adsorbed intermediates which is a common occurrence in noble metal-based CO2RR electrocatalysts. Typically, in conventional catalysts, CO_2 electroreduction activity decreases rapidly during high rate reactions because of catalysis agglomeration [65] change of active-phase composition [9, 66], and element dissolution [12, 67]. There have been very few studies where catalyst has been shown to be stable at commercially relevant current densities. To our knowledge, such extended functional stability for CO_2 electroreduction with continuous product formation for more than 50 h, has not been demonstrated by other electrocatalysts. Hence, CoTe exhibits an unprecedented activity and stability compared not only within the Co-based catalysts, but also to noble metal-based catalysts (Table S4). In order to achieve formate and acetic acid production from CO_2 in a practical yield, with the help of renewable power sources, it is critically necessary to develop catalysts that are not only active but also stable for prolonged period of operation. Various surface and bulk characterization techniques (morphological, structural, and compositional) were employed for tracking the integrity of the catalyst during CO2RR at different current densities and at different points of time. SEM images confirmed structural integrity and morphology retention after prolonged activity within potential range of -0.25 to -1.1 V vs RHE (Figure S3). Analysis of the catalyst surface after

prolonged CO2RR activity showed that the composition of CoTe crystalline phase was also retained as observed from the pxrd pattern which showed similarity with the as-synthesized sample (Figure S4). The robustness of the catalyst composition after prolonged activity was also confirmed through ICP-MS analysis of the electrolyte which showed that there was no Co and/or Te detected in the electrolyte after several hours of continuous CO2RR (Table S1). The ICP-MS analysis revealed that there was no catalyst leaching or degradation confirming compositional stability.

The reaction rates for different products at specific voltages have been estimated from NMR data and chronoamperometry measurement, as shown in Fig. 6a. To achieve better understanding about the selectivity and reaction kinetics, the production rates and partial current density for each product was estimated at different potentials. As shown in Fig. 6a, formic acid was major product at higher negative potentials contributing towards the CO2RR activity. Partial current density of the products was calculated from total current density and Faradaic efficiency of that product which was plotted as function of potential. Faradaic efficiency of formic acid in particular is affected by two factors: (1) concentration of protons in the vicinity of electrode; (2) the electric field near the electrode [68]. The high current density observed resulted in improved proton concentration near the electrodes, thereby increasing the rate of formate production. The formic acid partial current density has been used as a key parameter to determine the CO_2 -to-formate reduction activity and is calculated from FE of formate and total current density at different potentials on each sample (Fig. 6b). The formic acid
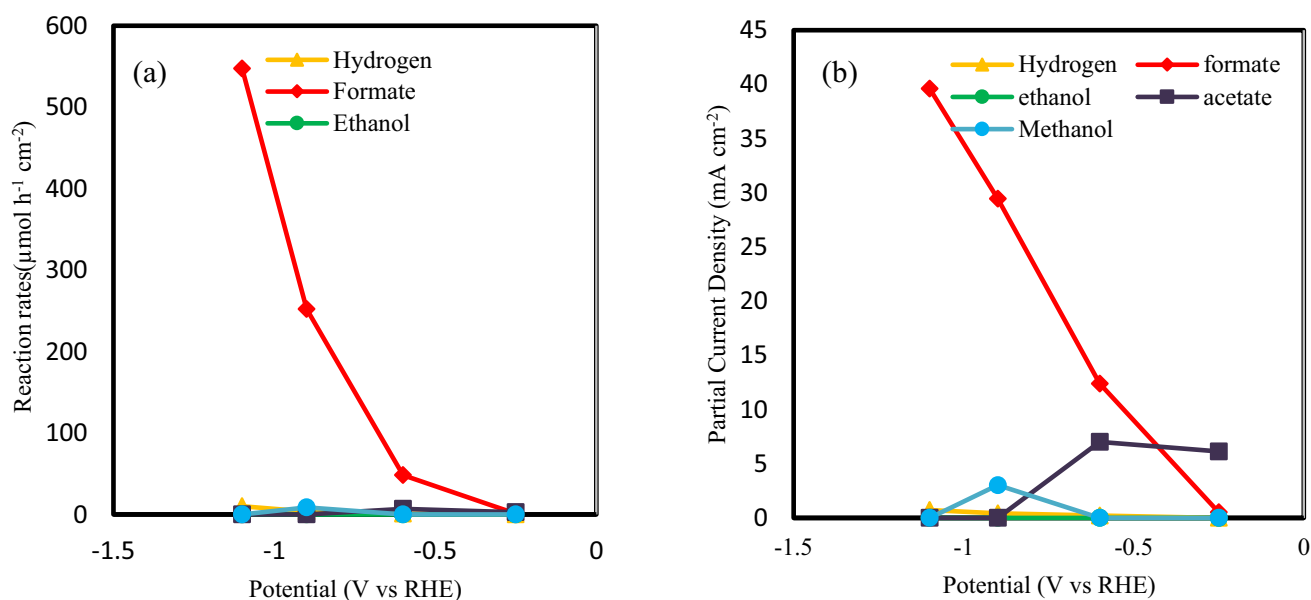

Fig. 6 **a** Formation rates of hydrogen, formate, ethanol, acetate, and methanol at various applied potential. **b** Partial current density of individual products, hydrogen, formate, ethanol, acetate, and methanol at specific potentials

partial current density of CoTe sample is higher than those of the bare Co and Co_3O_4 reported in other studies [28, 45], and reaches to the highest value of 58.6 mA cm^{-2} at an applied potential of -1.1 V vs RHE. This value is 11 and 93% higher than those reported for Co_3O_4 and Co, respectively [69]. At low negative potential, acetic acid exhibited higher production rate concurrent with the higher Faradaic efficiency. Acetic acid also exhibited higher current density at lower applied potential. Trends in current density and production rate confirms the selectivity towards specific products and also the uniqueness of this catalyst when compared with other Co-based CO_2 electroreduction catalysts which yields only C1 products. It must be noted that products quantification through NMR and GC-TCD measurements as well as estimation of formation rates for various products were repeated several times and Figs. 4, 5 and 6 represent the mean data. The plots with error bars have been included as Figure S5 and Figure S6 in supporting information, which indicates the reproducibility of results. Standard deviation from 3 trials was used to calculate the error bar. This CO2RR activity and higher preference towards formation of carbon-rich products can be attributed towards different rate of conversion for the adsorbed *CO (intermediate) on the surface, which in turn, is affected by the adsorption energy and dwell time of this intermediate *CO. Also, rate of decarboxylation and dehydroxylation at specific potentials can play a major role in CO2RR activity. The CO2RR activity achieved with CoTe indicates that this catalyst is capable of promoting CO_2 electrochemical conversion to yield significant quantities of value-added products with higher production rates over long period of time at lower applied potential.

Electrochemical capacitance measurements

Enhanced electrocatalytic activity can typically be assigned to intrinsic factors which includes facile catalyst activation through intermediate adsorption and enhanced charge transport, as well as extrinsic factors such as catalyst morphology and surface roughness which influences electrolyte and analyte access to the catalytically active sites. The extrinsic factors affecting CO2RR electrocatalytic activity of CoTe was investigated by estimating the electrochemically active surface area (ECSA) by following previously reported experimental procedure [70]. The ECSA was calculated by plotting electrochemical double layer capacitance in the non-Faradaic region as a function of scan rate and then comparing specific capacitance (C_S) to the double layer capacitance. The electrochemical double layer capacitance (C_{DL}) was calculated following equation:

$$i_{DL} = C_{DL} \times \nu, \tag{3}$$

where i_{DL} represents the current observed while ν is the scan rate. As can be seen from the Fig. 7, C_{DL} calculated from the i vs ν plot resulted in value of 0.5 mF.

The ratio of C_{DL} and Cs was used to calculate ECSA as shown in the following equation:

$$ECSA = C_{DL}/Cs. \tag{4}$$

Fig. 7 CV scans of CoTe@CFP from scan rate 5–200 mV s^{-1} over a potential range of 32 mV around the open circuit potential in 0.3 M NaHCO$_3$. Inset shows variation of anodic and cathodic current as function of scan rate at -0.12 V vs RHE
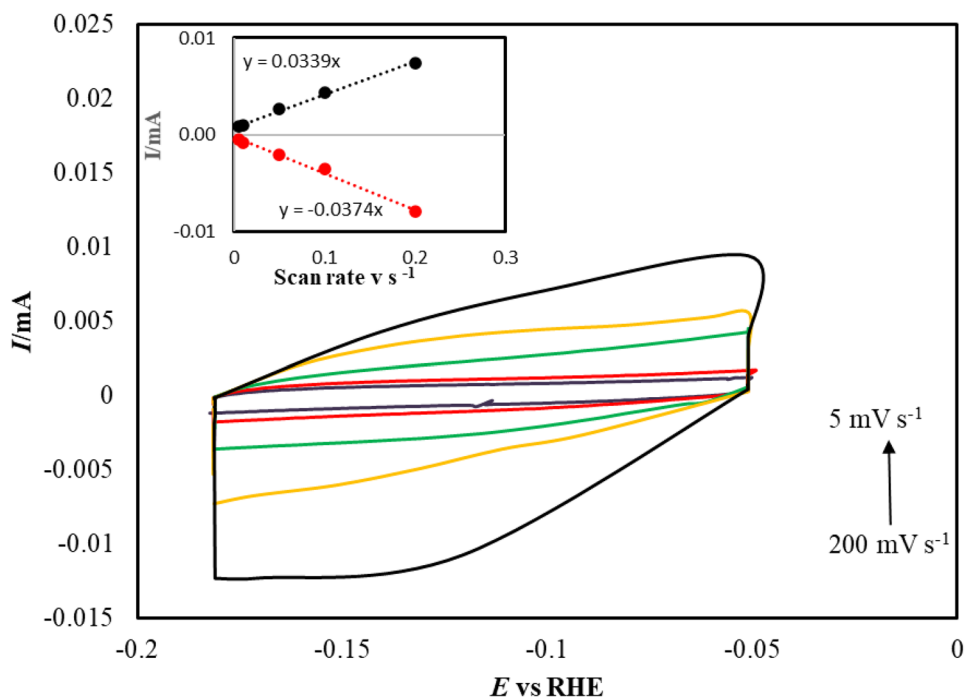
Cyclic voltammetry (CV) was used for the ECSA and roughness factor (RF) measurements. The cyclic voltammograms in CO_2 saturated 0.3 M $NaHCO_3$ were collected at scan rates from 5 to 400 mV/s. Polarization curves were obtained in potential range of 32 mV according to OCP of CoTe electrode. Current density from cyclic voltammograms was plotted as a function of scan rate. The surface roughness factor was calculated from the capacitance data. Using the Cs value (40 μF cm^{-2}) from reported values and C_{DL} value (0.0375 mF) from the plot, ECSA value was calculated to be 0.94 cm^2. The effect of catalyst morphology on the working electrode was also estimated from the RF which was calculated to be 11.75 from the ratio between ECSA and geometric electrode area (0.08 cm^2). High value of ECSA and RF depicts that CO_2 dissolved in the electrolyte has more access to the catalytic sites on working electrode, leading to better conversion efficiency. Few studies have claimed that CO_2 mass transfer is less in H-cell because of less solubility of CO_2 in electrolyte. This results in current density in the range of 0–50 mA cm^{-2} for CO_2 reduction [2, 17] The CO_2 mass transfer is expected to improve in flow cell set-up and use of such flow cell for CoTe may lead to suppression of hydrogen evolution resulting in higher faradaic efficiency for formic acid at higher negative potential along with higher current density (> 300 mA cm^{-2}).

Electrochemical impedance spectroscopy measurements

Impedance spectroscopy was used to gain insight into charge transfer kinetics on the working electrode during the electrochemical reaction. Electrochemical Impedance (EIS) was measured for CoTe-modified electrode in CO_2 saturated 0.3 M $NaHCO_3$ electrolyte to estimate the charge transfer resistance at the catalyst-analyte (electrolyte) interface and study its variance as a function of applied potential. Nyquist plots were measured at different negative potentials from −0.25 to −1.1 V vs RHE in frequency range of $1–10^5$ Hz in CO_2 purged $NaHCO_3$ solution as shown in Fig. 8. As the potential is decreased towards more negative potentials, modular values of the impedance decreased indicating that rate of electrochemical reaction increased on the electrode surface. EIS study was also conducted (Fig. 8b) with and without CO_2 purging (N_2 saturated) at a specific potential (−1.1 V) to show the difference in reaction kinetics between CO2RR and HER. CoTe was found to have lower impedance in CO_2 purged solution in comparison to N_2 purged solution which proves that CO2RR process is better facilitated than HER at this potential. The Nyquist plots were fitted using the equivalent circuit which consisted of electrode film resistance (R_s), charge transfer resistance at electrode–electrolyte interface (R_{CT}), and Warburg resistance. Table 1 shows the variation of R_s and R_{CT} at different applied potentials. It was observed that R_{CT} increased at lower applied potential indicating faster charge transfer and higher reaction rates for C_2 product formation at more cathodic potentials. Warburg impedance (W) associated with R_{CT} was also reported in Table 1 for efficient fitting of Nyquist plot. Lower values of Warburg resistance at higher negative potential implies that diffusion played a major role in enhancing CO2RR activity. Moreover, in CO_2-saturated electrolyte, both HER and CO2RR occur competitively at potentials lower than −0.4 V.
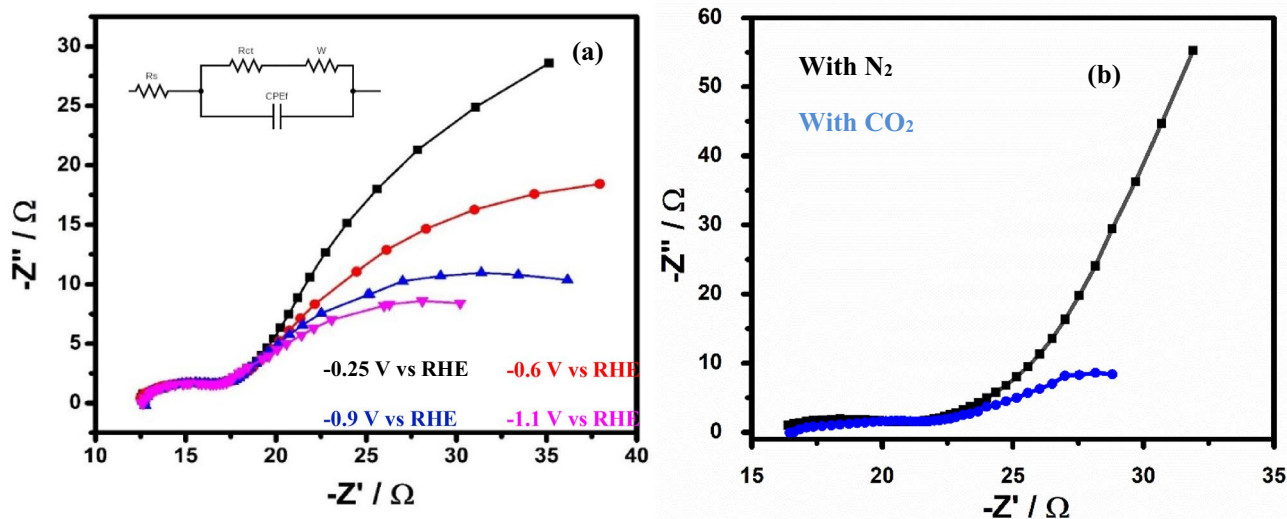

Fig. 8 a Nyquist plots of CoTe@CFP in CO_2-saturated 0.3 M $NaHCO_3$ electrolyte (pH 6.8) measured from 0 to −1.1 V vs RHE. Inset shows the equivalent circuit fitted to experimental spectra, where R_{CT} corresponds to the charge transfer resistance on cata-lyst-electrolyte interface, while R_s indicates film resistance of the catalyst composite. **b** Comparison of the Nyquist plot measured in CO_2-saturated (blue) and N_2-saturated electrolyte (black) illustrating the difference between CO2RR and HER, respectively

Parameters	Potential (V vs RHE)				
	− 1.1 with N_2 purging	− 1.1 with CO_2 purging	− 0.9 with CO_2 purging	− 0.6 with CO_2 purging	− 0.25 with CO_2 purging
R_s (Ω)	14.2	12.6	13.8	13.1	13.3
R_{CT} (Ω)	3.38	2.24	2.33	2.76	3.20
C (F)	5.70×10^{-6}	1.84×10^{-5}	1.04×10^{-5}	2.77×10^{-5}	1.79×10^{-5}
W (Ω)	6.42×10^{-3}	1.44×10^{-2}	1.45×10^{-2}	1.87×10^{-2}	1.95×10^{-2}

Table 1 Fitting parameters obtained from Nyquist plots at various potentials

The R_{CT} for the CoTe in the CO_2-staurated electrolyte (2.24 Ω) is smaller than that in the N_2-saturated medium (3.38 Ω), which indicates that CoTe is significantly more active for CO2RR compared to HER. Therefore, detailed EIS analysis confirms that the CoTe-modified electrode can exhibit significant improvement in selectivity for CO2RR supporting higher reaction rates and faster charge transfer.

CoTe lattice consists of chains of edge-shared $CoTe_6$ octahedra as shown in Figure S7 [24]. Such lattice structure leads to larger packing density of Co atoms on the lattice surface leading to larger anion deficiency with substantial unsaturation at the Co site on the surface. Such factors can lead to preferential adsorption of oxygenated intermediates on the catalytic site under lower electric field (i.e. lower applied potential). Moreover, Co being the catalytically active site, higher packing density of Co atoms also leads to significantly improved CO adsorption on the surface. Hence higher activity of CoTe towards CO2RR at low applied potential can be attributed to improved intermediate adsorption and larger anion deficiency. Previous research has also showed the effect of decreasing lattice anion electronegativity in improving the electrocatalytic activity [71]. Benchmarking of the CO2RR

activity of CoTe with other electrocatalysts reported by previous researchers confirm the novelty of this catalyst system as shown in Fig. 9. As can be seen from this comparison figure, CoTe shows a stark difference from other electrocatalysts since it can form acetic acid with high yield while other catalysts predominantly form CO and formic acid. Formation of such carbon-rich value-added industrially relevant hydrocarbon can lead to development of appropriate CO_2 utilization techniques that can eventually help to mitigate the catastrophic build-up of atmospheric CO_2. Figure 9 has been constructed compiling results from various reports published by researchers worldwide, and the complementary list of the references used has been reported in the supporting information.

Conclusion

CO2RR gives us a hope to develop a carbon neutral way of living where electrochemical reduction can convert CO_2 into valuable chemicals leading to efficient CO_2 utilization. In this study, we have reported successful one-step
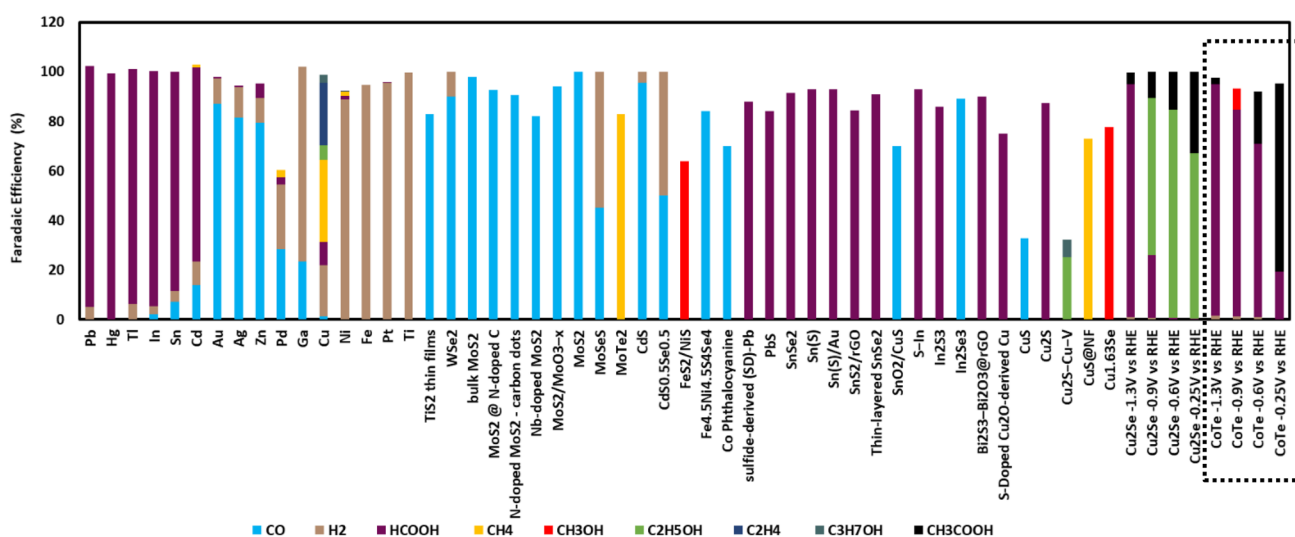

Fig. 9 Comprehensive comparison of products obtained through electrocatalytic CO2RR with CoTe (boxed region) and other catalysts as assembled from various reports published from different research groups

synthesis of CoTe, which can be used as efficient electrocatalyst for CO_2 reduction. The as-prepared CoTe catalyst showed enhanced catalytic performance for electroreduction CO_2 to acetic acid with high FE of 87% at low potential of -0.25 V vs RHE. At higher cathodic potentials, formic acid was obtained as major product with high FE and high partial current density of 12.40 mA cm^{-2} at -0.6 V vs RHE. It must be noted that the potentials required for CO_2 reduction with CoTe-modified electrode was the lowest among other Co-based catalyst. The formation rate of formic acid reached a high value of 547.24 µmol cm^{-2} h^{-1}, which was comparable to other excellent electrocatalysts reported previously. Moreover, CoTe is the only Co-based catalyst that exhibits high preference for formation of carbon-rich products increasing the novelty of this system. This enhanced performance and selectivity can be due to various extrinsic and intrinsic factors like large ECSA and high density of catalytically active sites, faster charge transfer, larger lattice covalency resulting in optimum stabilization of the intermediate *CO* and better interaction between the catalytically active sites and the OCHO· intermediate. In summary, the CoTe electrocatalyst deposited on carbon fiber paper is first cobalt-based catalyst which can produce acetic acid from reduction of CO_2 under ambient condition. This catalyst shows high current density of 40.33 mA cm^{-2} for extended period of time. Robustness of this catalyst composition can be attributed to the increased covalency of the Co–Te bond which inhibits tellurium leaching and catalyst degradation during CO2RR. This catalyst is uniquely selective and energy efficient since it can produce acetic acid with high yield (FE = 87%) at very low potential (-0.25 V vs RHE). while formic acid forms exclusively at higher negative potential (-1.1 V) with FE of 93.39% and with high formation rate (547.24 µmol cm^{-2} h^{-1}). These results provide a significant advancement in CO_2 utilization research focus by providing novel compositions that can lead to selective formation of value-added product as well as offer functional stability for prolonged period.

Declarations

References

1. Mikkelsen, M., Jørgensen, M., Krebs, F.C.: The teraton challenge. A review of fixation and transformation of carbon dioxide. Energy Environ. Sci. **3**, 43–81 (2010). https://doi.org/10.1039/B912904A

2. Spinner, N.S., Vega, J.A., Mustain, W.E.: Recent progress in the electrochemical conversion and utilization of CO_2. Catal. Sci. Technol. **2**, 19–28 (2011). https://doi.org/10.1039/C1CY00314C

3. Zhu, D.D., Liu, J.L., Qiao, S.Z.: Recent advances in inorganic heterogeneous electrocatalysts for reduction of carbon dioxide. Adv. Mater. **28**, 3423–3452 (2016). https://doi.org/10.1002/ADMA.201504766

4. Li, C.W., Ciston, J., Kanan, M.W.: Electroreduction of carbon monoxide to liquid fuel on oxide-derived nanocrystalline copper. Nature **508**, 504–507 (2014). https://doi.org/10.1038/nature13249

5. Boutin, E., Merakeb, L., Ma, B., Boudy, B., Wang, M., Bonin, J., Anxolabéhère-Mallart, E., Robert, M.: Molecular catalysis of CO_2 reduction: recent advances and perspectives in electrochemical and light-driven processes with selected Fe, Ni and Co aza macrocyclic and polypyridine complexes. Chem. Soc. Rev. **49**, 5772–5809 (2020). https://doi.org/10.1039/D0CS00218F

6. Nath, M., Singh, H., Saxena, A.: Progress of transition metal chalcogenides as efficient electrocatalysts for energy conversion. Curr. Opin. Electrochem. (2022). https://doi.org/10.1016/J.COELEC.2022.100993

7. Li, K., Peng, B., Peng, T.: Recent advances in heterogeneous photocatalytic CO_2 conversion to solar fuels. ACS Catal. **6**, 7485–7527 (2016). https://doi.org/10.1021/ACSCATAL.6B02089

8. Hori, Y., Wakebe, H., Tsukamoto, T., Koga, O.: Electrocatalytic process of CO selectivity in electrochemical reduction of CO_2 at metal electrodes in aqueous media. Electrochim. Acta. **39**, 1833–1839 (1994). https://doi.org/10.1016/0013-4686(94)85172-7

9. Ye, K., Zhou, Z., Shao, J., Lin, L., Gao, D., Ta, N., Si, R., Wang, G., Bao, X.: In situ reconstruction of a hierarchical Sn–Cu/SnO$_x$ core/shell catalyst for high-performance CO_2 electroreduction. Angew. Chemie Int. Ed. **59**, 4814–4821 (2020). https://doi.org/10.1002/ANIE.201916538

10. Han, N., Wang, Y., Yang, H., Deng, J., Wu, J., Li, Y., Li, Y.: Ultrathin bismuth nanosheets from in situ topotactic transformation for selective electrocatalytic CO_2 reduction to formate. Nat. Commun. **9**, 1–8 (2018). https://doi.org/10.1038/s41467-018-03712-z

11. Wang, Z., Qi, R., Liu, D., Zhao, X., Huang, L., Chen, S., Chen, Z., Li, M., You, B., Pang, Y., Yu Xia, B.: Exfoliated ultrathin ZnIn$_2$S$_4$ nanosheets with abundant zinc vacancies for enhanced CO_2 electroreduction to formate. Chemsuschem **14**, 852–859 (2021). https://doi.org/10.1002/CSSC.202002785

12. Zhou, J.H., Yuan, K., Zhou, L., Guo, Y., Luo, M.Y., Guo, X.Y., Meng, Q.Y., Zhang, Y.W.: Boosting electrochemical reduction of CO_2 at a low overpotential by amorphous Ag–Bi–S–O decorated Bi0 nanocrystals. Angew. Chemie Int. Ed. **58**, 14197–14201 (2019). https://doi.org/10.1002/ANIE.201908735

13. Ma, W., Xie, S., Zhang, X.G., Sun, F., Kang, J., Jiang, Z., Zhang, Q., Wu, D.Y., Wang, Y.: Promoting electrocatalytic CO_2 reduction

to formate via sulfur-boosting water activation on indium surfaces. Nat. Commun. **10**, 1–10 (2019). https://doi.org/10.1038/s41467-019-08805-x

14. Grigioni, I., Sagar, L.K., Li, Y.C., Lee, G., Yan, Y., Bertens, K., Miao, R.K., Wang, X., Abed, J., Won, D.H., Garciá De Arquer, F.P., Ip, A.H., Sinton, D., Sargent, E.H.: CO_2 electroreduction to formate at a partial current density of 930 mA cm$^{−2}$ with InP colloidal quantum dot derived catalysts. ACS Energy Lett. **6**, 79–84 (2021). https://doi.org/10.1021/ACSENERGYLETT.0C02165/SUPPL_FILE/NZ0C02165_SI_001.PDF

15. Zheng, X., De Luna, P., García de Arquer, F.P., Zhang, B., Becknell, N., Ross, M.B., Li, Y., Banis, M.N., Li, Y., Liu, M., Voznyy, O., Dinh, C.T., Zhuang, T., Stadler, P., Cui, Y., Du, X., Yang, P., Sargent, E.H.: Sulfur-modulated tin sites enable highly selective electrochemical reduction of CO_2 to formate. Joule **1**, 794–805 (2017). https://doi.org/10.1016/J.JOULE.2017.09.014/ATTACHMENT/557349C1-9E4C-413A-A15A-52D4DCDF1A6E/MMC1.PDF

16. Kuhl, K.P., Cave, E.R., Abram, D.N., Jaramillo, T.F.: New insights into the electrochemical reduction of carbon dioxide on metallic copper surfaces. Energy Environ. Sci. **5**, 7050–7059 (2012). https://doi.org/10.1039/C2EE21234J

17. Saxena, A., Liyanage, W., Masud, J., Kapila, S., Nath, M.: Selective electroreduction of CO_2 to carbon-rich products with a simple binary copper selenide electrocatalyst. J. Mater. Chem. A. **9**, 7150–7161 (2021). https://doi.org/10.1039/D0TA11518E

18. Abdinejad, M., Mirza, Z., Zhang, X.A., Kraatz, H.B.: Enhanced electrocatalytic activity of primary amines for CO_2 reduction using copper electrodes in aqueous solution. ACS Sustain. Chem. Eng. **8**, 1715–1720 (2020). https://doi.org/10.1021/ACSSUSCHEMENG.9B06837/SUPPL_FILE/SC9B06837_SI_001.PDF

19. Bernal, M., Bagger, A., Scholten, F., Sinev, I., Bergmann, A., Ahmadi, M., Rossmeisl, J., Cuenya, B.R.: CO_2 electroreduction on copper-cobalt nanoparticles: size and composition effect. Nano Energy **53**, 27–36 (2018). https://doi.org/10.1016/J.NANOEN.2018.08.027

20. Saxena, A., Liyanage, W., Kapila, S., Nath, M.: Nickel selenide as efficient electrocatalyst for selective reduction of carbon dioxide to carbon-rich products. Catal. Sci. Technol. (2022). https://doi.org/10.1039/D2CY00583B

21. Richard, L.A., Moreau, P., Rugmini, S., Daly, F.: Fischer–Tropsch performance correlated to catalyst structure: trends in activity and stability for a silica-supported cobalt catalyst. Appl. Catal. A Gen. **464–465**, 200–206 (2013). https://doi.org/10.1016/J.APCATA.2013.05.047

22. Fischer, N., Van Steen, E., Claeys, M.: Structure sensitivity of the Fischer–Tropsch activity and selectivity on alumina supported cobalt catalysts. J. Catal. **299**, 67–80 (2013). https://doi.org/10.1016/J.JCAT.2012.11.013

23. Arde, P., Ramanjaneyulu, B.T., Reddy, V., Saxena, A., Anand, R.V.: *N*-Heterocyclic carbene catalysed aerobic oxidation of aromatic aldehydes to aryl esters using boronic acids. Org. Biomol. Chem. **10**, 848–851 (2012). https://doi.org/10.1039/C1OB06566A

24. Nath, M., De Silva, U., Singh, H., Perkins, M., Liyanage, W.P.R., Umapathi, S., Chakravarty, S., Masud, J.: Cobalt telluride: a highly efficient trifunctional electrocatalyst for water splitting and oxygen reduction. ACS Appl. Energy Mater. **4**, 8158–8174 (2021). https://doi.org/10.1021/ACSAEM.1C01438/SUPPL_FILE/AE1C01438_SI_001.PDF

25. Guo, Y., Wang, Y., Shen, Y., Cai, Z., Li, Z., Liu, J., Chen, J., Xiao, C., Liu, H., Lin, W., Wang, C.: Tunable cobalt-polypyridyl catalysts supported on metal-organic layers for electrochemical CO_2 reduction at low overpotentials. J. Am. Chem. Soc. **142**, 21493–21501 (2020). https://doi.org/10.1021/JACS.0C10719/SUPPL_FILE/JA0C10719_SI_001.PDF

26. Geng, Z., Cao, Y., Chen, W., Kong, X., Liu, Y., Yao, T., Lin, Y.: Regulating the coordination environment of Co single atoms for achieving efficient electrocatalytic activity in CO_2 reduction. Appl. Catal. B Environ. **240**, 234–240 (2019). https://doi.org/10.1016/J.APCATB.2018.08.075

27. Hou, P., Song, W., Wang, X., Hu, Z., Kang, P.: Well-defined single-atom cobalt catalyst for electrocatalytic flue gas CO_2 reduction. Small **16**, 2001896 (2020). https://doi.org/10.1002/smll.202001896

28. Gao, S., Lin, Y., Jiao, X., Sun, Y., Luo, Q., Zhang, W., Li, D., Yang, J., Xie, Y.: Partially oxidized atomic cobalt layers for carbon dioxide electroreduction to liquid fuel. Nature **529**, 68–71 (2016). https://doi.org/10.1038/nature16455

29. Zhang, S.Y., Yang, Y.Y., Zheng, Y.Q., Zhu, H.L.: Ag-doped Co_3O_4 catalyst derived from heterometallic MOF for syngas production by electrocatalytic reduction of CO_2 in water. J. Solid State Chem. **263**, 44–51 (2018). https://doi.org/10.1016/J.JSSC.2018.04.007

30. Matheu, R., Gutierrez-Puebla, E., Monge, M.Á., Diercks, C.S., Kang, J., Prévot, M.S., Pei, X., Hanikel, N., Zhang, B., Yang, P., Yaghi, O.M.: Three-dimensional phthalocyanine metal-catecholates for high electrochemical carbon dioxide reduction. J. Am. Chem. Soc. **141**, 17081–17085 (2019). https://doi.org/10.1021/JACS.9B09298/SUPPL_FILE/JA9B09298_SI_003.CIF

31. Long, D., Li, X., Yin, Z., Fan, S., Wang, P., Xu, F., Wei, L., Tadé, M.O., Liu, S.: Novel Co_3O_4 @ $CoFe_2O_4$ double-shelled nanoboxes derived from metal-organic framework for CO_2 reduction. J. Alloys Compd. **854**, 156942 (2021). https://doi.org/10.1016/J.JALLCOM.2020.156942

32. Lin, S., Diercks, C.S., Zhang, Y.B., Kornienko, N., Nichols, E.M., Zhao, Y., Paris, A.R., Kim, D., Yang, P., Yaghi, O.M., Chang, C.J.: Covalent organic frameworks comprising cobalt porphyrins for catalytic CO_2 reduction in water. Science (80-) **349**, 1208–1213 (2015). https://doi.org/10.1126/SCIENCE.AAC8343/SUPPL_FILE/LIN.SM.PDF

33. Huang, P., Huang, J., Pantovich, S.A., Carl, A.D., Fenton, T.G., Caputo, C.A., Grimm, R.L., Frenkel, A.I., Li, G.: Selective CO_2 reduction catalyzed by single cobalt sites on carbon nitride under visible-light irradiation. J. Am. Chem. Soc. **140**, 16042–16047 (2018). https://doi.org/10.1021/JACS.8B10380/SUPPL_FILE/JA8B10380_SI_001.PDF

34. Fu, J., Zhu, L., Jiang, K., Liu, K., Wang, Z., Qiu, X., Li, H., Hu, J., Pan, H., Lu, Y.R., Chan, T.S., Liu, M.: Activation of CO_2 on graphitic carbon nitride supported single-atom cobalt sites. Chem. Eng. J. **415**, 128982 (2021). https://doi.org/10.1016/J.CEJ.2021.128982

35. Di, J., Chen, C., Zhu, C., Song, P., Duan, M., Xiong, J., Long, R., Xu, M., Kang, L., Guo, S., Chen, S., Chen, H., Chi, Z., Weng, Y.X., Li, H., Song, L., Wu, M., Yan, Q., Li, S., Liu, Z.: Cobalt nitride as a novel cocatalyst to boost photocatalytic CO_2 reduction. Nano Energy **79**, 105429 (2021). https://doi.org/10.1016/J.NANOEN.2020.105429

36. Gao, S., Jiao, X., Sun, Z., Zhang, W., Sun, Y., Wang, C., Hu, Q., Zu, X., Yang, F., Yang, S., Liang, L., Wu, J., Xie, Y.: Ultrathin Co_3O_4 layers realizing optimized CO_2 electroreduction to formate. Angew. Chemie. **128**, 708–712 (2016). https://doi.org/10.1002/ANGE.201509800

37. Cheng, Y., Veder, J.P., Thomsen, L., Zhao, S., Saunders, M., Demichelis, R., Liu, C., De Marco, R., Jiang, S.P.: Electrochemically substituted metal phthalocyanines, e-MPc (M = Co, Ni), as highly active and selective catalysts for CO_2 reduction. J. Mater. Chem. A. **6**, 1370–1375 (2018). https://doi.org/10.1039/C7TA09208C

38. Yadav, V.S.K., Purkait, M.K.: Electrochemical studies for CO_2 reduction using synthesized Co_3O_4 (anode) and Cu_2O (cathode) as electrocatalysts. Energy Fuels **29**, 6670–6677 (2015). https://doi.org/10.1021/ACS.ENERGYFUELS.5B01656

39. Guo, S., Zhao, S., Wu, X., Li, H., Zhou, Y., Zhu, C., Yang, N., Jiang, X., Gao, J., Bai, L., Liu, Y., Lifshitz, Y., Lee, S.T., Kang, Z.: A Co_3O_4-CDots-C_3N_4 three component electrocatalyst design concept for efficient and tunable CO_2 reduction to syngas. Nat. Commun. **8**, 1–9 (2017). https://doi.org/10.1038/s41467-017-01893-7

40. Nguyen, D.T., Nguyen, C.C., Do, T.O.: Rational one-step synthesis of cobalt clusters embedded-graphitic carbon nitrides for the efficient photocatalytic CO_2 reduction under ambient conditions. J. Catal. **392**, 88–96 (2020). https://doi.org/10.1016/J.JCAT.2020.09.038

41. Li, C., Tong, X., Yu, P., Du, W., Wu, J., Rao, H., Wang, Z.M.: Carbon dioxide photo/electroreduction with cobalt. J. Mater. Chem. A. **7**, 16622–16642 (2019). https://doi.org/10.1039/C9TA03892B

42. Yang, P., Wang, R., Tao, H., Zhang, Y., Titirici, M.M., Wang, X.: Cobalt nitride anchored on nitrogen-rich carbons for efficient carbon dioxide reduction with visible light. Appl. Catal. B Environ. **280**, 119454 (2021). https://doi.org/10.1016/J.APCATB.2020.119454

43. Huang, J., Guo, X., Yue, G., Hu, Q., Wang, L.: Boosting CH_3OH production in electrocatalytic CO_2 reduction over partially oxidized 5 nm cobalt nanoparticles dispersed on single-layer nitrogen-doped graphene. ACS Appl. Mater. Interfaces. **10**, 44403–44414 (2018). https://doi.org/10.1021/ACSAMI.8B14822/SUPPL_FILE/AM8B14822_SI_001.PDF

44. Shi, L., Ren, X., Wang, Q., Li, Y., Ichihara, F., Zhang, H., Izumi, Y., Ren, L., Zhou, W., Yang, Y., Ye, J.: Stabilizing atomically dispersed catalytic sites on tellurium nanosheets with strong metal-support interaction boosts photocatalysis. Small **16**, 2002356 (2020). https://doi.org/10.1002/SMLL.202002356

45. Aljabour, A., Coskun, H., Apaydin, D.H., Ozel, F., Hassel, A.W., Stadler, P., Sariciftci, N.S., Kus, M.: Nanofibrous cobalt oxide for electrocatalysis of CO_2 reduction to carbon monoxide and formate in an acetonitrile-water electrolyte solution. Appl. Catal. B Environ. **229**, 163–170 (2018). https://doi.org/10.1016/J.APCATB.2018.02.017

46. Wang, M., Torbensen, K., Salvatore, D., Ren, S., Joulié, D., Dumoulin, F., Mendoza, D., Lassalle-Kaiser, B., Işci, U., Berlinguette, C.P., Robert, M.: CO_2 electrochemical catalytic reduction with a highly active cobalt phthalocyanine. Nat. Commun. **10**, 1–8 (2019). https://doi.org/10.1038/s41467-019-11542-w

47. Yan, Y., Li, K., Chen, X., Yang, Y., Lee, J.M.: Heterojunction-assisted Co_3S_4@Co_3O_4 core-shell octahedrons for supercapacitors and both oxygen and carbon dioxide reduction reactions. Small **13**, 1701724 (2017). https://doi.org/10.1002/SMLL.201701724

48. Chernyshova, I.V., Somasundaran, P., Ponnurangam, S.: On the origin of the elusive first intermediate of CO_2 electroreduction. Proc. Natl. Acad. Sci. USA **115**, E9261–E9270 (2018). https://doi.org/10.1073/PNAS.1802256115/SUPPL_FILE/PNAS.1802256115.SAPP.PDF

49. Singh, H., Bernabe, J., Chern, J., Nath, M.: Copper selenide as multifunctional non-enzymatic glucose and dopamine sensor. J. Mater. Res. **36**, 1413–1424 (2021). https://doi.org/10.1557/S43578-021-00227-0

50. Singh, H., Marley-Hines, M., Chakravarty, S., Nath, M.: Multi-walled carbon nanotube supported manganese selenide as highly active bifunctional OER and ORR electrocatalyst. J. Mater. Chem. A. **6**, 4883–5230 (2022). https://doi.org/10.1039/D1TA09864K

51. Umapathi, S., Singh, H., Masud, J., Nath, M.: Nanostructured copper selenide as an ultrasensitive and selective non-enzymatic glucose sensor. Mater. Adv. (2020). https://doi.org/10.1039/D0MA00890G

52. Amin, B.G., Masud, J., Nath, M.: Facile one-pot synthesis of $NiCo_2Se_4$-rGO on Ni foam for high performance hybrid supercapacitors. RSC Adv. **9**, 37939–37946 (2019). https://doi.org/10.1039/c9ra06439g

53. Kim, B., Hillman, F., Ariyoshi, M., Fujikawa, S., Kenis, P.J.A.: Effects of composition of the micro porous layer and the substrate on performance in the electrochemical reduction of CO_2 to CO. J. Power Sources. **312**, 192–198 (2016). https://doi.org/10.1016/J.JPOWSOUR.2016.02.043

54. Lei, Y.X., Miao, N.X., Zhou, J.P., Hassan, Q.U., Wang, J.Z.: Novel magnetic properties of CoTe nanorods and diversified $CoTe_2$ nanostructures obtained at different NaOH concentrations. Sci. Technol. Adv. Mater. **18**, 325–333 (2017). https://doi.org/10.1080/14686996.2017.1317218

55. Clark, E.L., Resasco, J., Landers, A., Lin, J., Chung, L.T., Walton, A., Hahn, C., Jaramillo, T.F., Bell, A.T.: Standards and protocols for data acquisition and reporting for studies of the electrochemical reduction of carbon dioxide. ACS Catal. **8**, 6560–6570 (2018). https://doi.org/10.1021/ACSCATAL.8B01340/SUPPL_FILE/CS8B01340_SI_001.PDF

56. Kottakkat, T., Klingan, K., Jiang, S., Jovanov, Z.P., Davies, V.H., El-Nagar, G.A.M., Dau, H., Roth, C.: Electrodeposited AgCu foam catalysts for enhanced reduction of CO_2 to CO. ACS Appl. Mater. Interfaces. **11**, 14734–14744 (2019). https://doi.org/10.1021/ACSAMI.8B22071/SUPPL_FILE/AM8B22071_SI_001.PDF

57. Qiu, W., Liang, R., Luo, Y., Cui, G., Qiu, J., Sun, X.: A Br$^-$ anion adsorbed porous Ag nanowire film: in situ electrochemical preparation and application toward efficient CO_2 electroreduction to CO with high selectivity. Inorg. Chem. Front. **5**, 2238–2241 (2018). https://doi.org/10.1039/C8QI00500A

58. Yu, Y., Zhong, N., Fang, J., Tang, S., Ye, X., He, Z., Song, S.: Comparative study between pristine Ag and Ag foam for electrochemical synthesis of syngas with carbon dioxide and water. Catalysts **9**, 57 (2019). https://doi.org/10.3390/CATAL9010057

59. Zhao, Y., Liang, J., Wang, C., Ma, J., Wallace, G.G.: Tunable and efficient tin modified nitrogen-doped carbon nanofibers for electrochemical reduction of aqueous carbon dioxide. Adv. Energy Mater. **8**, 1702524 (2018). https://doi.org/10.1002/aenm.201702524

60. Hori, Y.: Electrochemical CO_2 reduction on metal electrodes. In: Vayenas, C.G., White, R.E., Gamboa-Aldeco, M.E. (eds) Modern Aspects of Electrochemistry. Modern Aspects of Electrochemistry, vol 42. Springer, New York, NY. https://doi.org/10.1007/978-0-387-49489-0_3

61. Grim, R.G., Huang, Z., Guarnieri, M.T., Ferrell, J.R., Tao, L., Schaidle, J.A.: Transforming the carbon economy: challenges and opprtunities in the convergence of low-cost electricity and reductive CO_2 utilization. Energy Environ. Sci. **13**, 472–494 (2020). https://doi.org/10.1039/C9EE02410G

62. Tan, D., Cui, C., Shi, J., Luo, Z., Zhang, B., Tan, X., Han, B., Zheng, L., Zhang, J., Zhang, J.: Nitrogen-carbon layer coated nickel nanoparticles for efficient electrocatalytic reduction of carbon dioxide. Nano Res. **12**, 1167–1172 (2019). https://doi.org/10.1007/s12274-019-2372-1

63. The Cativa^TM Process for the Manufacture of Acetic Acid | Johnson Matthey Technology Review. (n.d.). https://www.technology.matthey.com/article/44/3/94-105/. Accessed 18 Nov 2021

64. Yang, H., Lin, Q., Zhang, C., Yu, X., Cheng, Z., Li, G., Hu, Q., Ren, X., Zhang, Q., Liu, J., He, C.: Carbon dioxide electroreduction on single-atom nickel decorated carbon membranes with industry compatible current densities. Nat. Commun. **11**, 1–8 (2020). https://doi.org/10.1038/s41467-020-14402-0

65. Wu, J., Sun, S.G., Zhou, X.D.: Origin of the performance degradation and implementation of stable tin electrodes for the conversion of CO_2 to fuels. Nano Energy **27**, 225–229 (2016). https://doi.org/10.1016/J.NANOEN.2016.06.028

66. Shi, Y., Ji, Y., Long, J., Liang, Y., Liu, Y., Yu, Y., Xiao, J., Zhang, B.: Unveiling hydrocerussite as an electrochemically stable active phase for efficient carbon dioxide electroreduction to formate. Nat. Commun. **11**, 1–10 (2020). https://doi.org/10.1038/s41467-020-17120-9

67. Cheng, H., Liu, S., Zhang, J., Zhou, T., Zhang, N., Zheng, X.S., Chu, W., Hu, Z., Wu, C., Xie, Y.: surface nitrogen-injection engineering for high formation rate of CO_2 reduction to formate. Nano Lett. **20**, 6097–6103 (2020). https://doi.org/10.1021/ACS.NANOLETT.0C02144/SUPPL_FILE/NL0C02144_SI_001.PDF

68. Wu, J., Sharma, P.P., Harris, B.H., Zhou, X.D.: Electrochemical reduction of carbon dioxide: IV dependence of the Faradaic efficiency and current density on the microstructure and thickness of tin electrode. J. Power Sources. **258**, 189–194 (2014). https://doi.org/10.1016/J.JPOWSOUR.2014.02.014

69. Usman, M., Humayun, M., Garba, M.D., Ullah, L., Zeb, Z., Helal, A., Suliman, M.H., Alfaifi, B.Y., Iqbal, N., Abdinejad, M., Tahir, A.A., Ullah, H.: Electrochemical reduction of CO_2: a review of cobalt based catalysts for carbon dioxide conversion to fuels. Nanomaterials **11**, 2029 (2021). https://doi.org/10.3390/NANO11082029

70. Masud, J., Liyanage, W.P.R., Cao, X., Saxena, A., Nath, M.: Copper selenides as high-efficiency electrocatalysts for oxygen evolution reaction. ACS Appl. Energy Mater. (2018). https://doi.org/10.1021/acsaem.8b00746

71. Suntivich, J., May, K.J., Gasteiger, H.A., Goodenough, J.B., Shao-Horn, Y.: A perovskite oxide optimized for oxygen evolution catalysis from molecular orbital principles. Science (80-) **334**, 1383–1385 (2011). https://doi.org/10.1126/SCIENCE.1212858/SUPPL_FILE/SUNTIVICH.SOM.PDF

Publisher's Note Springer Nature remains neutral with regard to jurisdictional claims in published maps and institutional affiliations.